Analysis of photon emission from 50–350-keV proton impact on H_2O

Benjamin D. Goldman, Stephanie A. Timpone, Michael N. Monce, Laurel Mitchell, and Brian Griffin
Daghlian Accelerator Laboratory, Department of Physics, Astronomy, and Geophysics, Connecticut College, New London, Connecticut 06320, USA
(Received 9 January 2011; published 4 April 2011)

We have measured photon emission cross sections from neutral fragments produced by collisions of 50–350 keV protons with H_2O molecules. Balmer $\alpha-\delta$ emissions from both the target and projectile were recorded. We also analyzed $A\,^2\Sigma^+ - X\,^2\Pi$ (0,0) and (1,0) emission from the excited OH fragment produced during target dissociation. Trends in the cross sections revealed two key properties of the collision process: (1) The Bethe theory accurately describes target emission from both H and OH fragments and (2) the ratio of any two Balmer emission cross sections for both the target and projectile can be approximated by simple functions of the respective optical oscillator strengths. Finally, we provide the Bethe fit parameters necessary to calculate the target emission cross sections at all nonrelativistic impact energies.

DOI: 10.1103/PhysRevA.83.042701 PACS number(s): 34.50.−s, 34.70.+e, 32.30.−r

I. INTRODUCTION

The cross sections for excitation and ionization of molecules by proton impact are of great interest in areas of applied physics, especially with regard to radiation damage of tissues and biomolecules [1]. In the planetary sciences the photon emission cross section may be of use when analyzing ionic phenomena within the atmospheres of planets. In 2006, Galand and Chakrabarti [2] reported a signature of kilo-electron-volt proton precipitation from the ionosphere of Earth, concluding that the presence of Doppler-shifted $H\alpha$ and $H\beta$ lines indicated electron capture of ionospheric species by protons. It was also determined that Balmer emission cross sections from proton impact with molecules such as O_2 and N_2 are needed to better understand proton beams at high altitudes. The cross sections measured in this work would therefore apply to planetary atmospheres containing or interacting with H_2O molecules in some form. A recent report by Moore *et al.* [3] indicated a flux of water vapor from the rings of Saturn into its upper ionosphere, which was directly observed by the Cassini spacecraft. They concluded that charge transfer from water molecules to protons may be acting as a proton depletion mechanism. It has also been noted that the protons with energies in the kilo-electron-volt range are responsible for this depletion [4]. Following from the conclusions of Galand and Chakrabarti, we should then be able to observe and interpret Doppler-shifted Balmer lines from these processes on Saturn. The photon emission cross sections could then be used in the further analysis of water fluxes in support of the recent results from Cassini.

In our previous work [5] we reported on cross sections from proton impact with H_2O at a single energy of 200 keV. In this paper we show the energy dependence of both the target emission cross sections and the projectile emission cross sections due to electron capture (charge transfer). There have been previous investigations of proton-H_2O collisions, providing a range of cross-section measurements for total ionization [6], partial ionization [7], and singly differential electron ejection [8]. Rarely have investigators reported on emission from neutral fragments of H_2O. Yousif *et al.* [9], were the first to report on the $H\alpha$ emission cross section for protons impacting on an H_2O target, while Nussbaum and Cathers [10] reported on $A\,^2\Sigma^+ - X\,^2\Pi$ (0,0) 315 nm emission from the excited OH fragment. Here we present cross-section measurements for the complete visible Balmer emission spectrum and ultraviolet OH emission spectrum from collisions of protons with H_2O over a large energy range.

II. EXPERIMENTAL DETAIL

The experimental setup and methods were generally the same as those used in our earlier work [5]. Using a Pelletron accelerator, we produced a proton beam collimated to a diameter of 3 mm incident on a differentially pumped target chamber, with regulated gas pressure kept under single-collision conditions. Beam current was measured using a Faraday cup and emitted photons were detected using a calibrated CCD. Photon count distributions were integrated to determine the total emission for each process. Figure 1 illustrates how the two Balmer emission processes were distinguished from one another. Projectile emissions due to charge transfer are Doppler-shifted to shorter wavelengths, with line intensities and shapes that are also distinctly different from the corresponding target Balmer line.

Before analyzing emission from the water molecule, we first verified the calibration of our setup for the expanded energy range. To accomplish this we determined the cross sections for the well-studied 391.2 nm emission line of N_2^+. A comparison to the cross sections compiled by Thomas [11] showed very good agreement.

Measurements in this work required some additional modifications to the procedures in Ref. [5] due to the expanded energy range. Two additional corrections to the data were applied. First, we corrected for proton neutralization due to gas leakage up the beam line. Especially at lower energies some of the incoming protons are neutralized from electron capture processes occurring before the target interaction region. The attenuation is as much as 40% at 50 keV and 8% at 350 keV. The second correction applies to the projectile emission cross section only. In our previous work using an SO_2 target [12], we determined the projectile emission cross-section correction, which takes into account the projectile velocity, excited

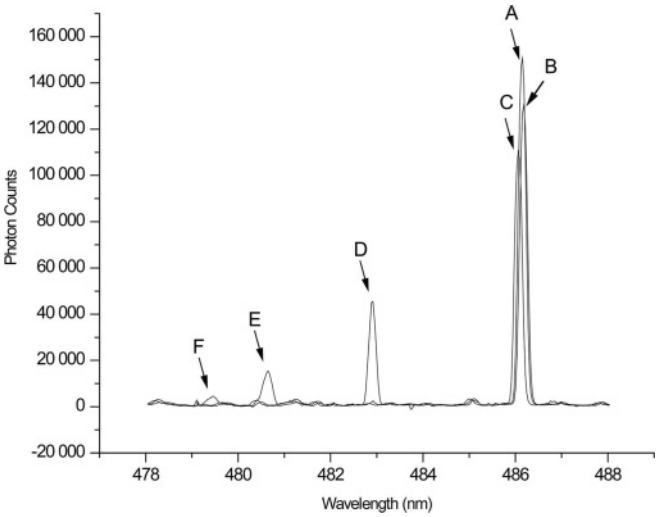

FIG. 1. A portion of the Balmer emission spectrum showing the $H\beta$ lines for 3 different projectile energies (plots superimposed on one another for comparison purposes). Points A–C identify the primary $H\beta$ lines for energies of 50, 150, and 225 keV, respectively. Points D–F identify the Doppler-shifted $H\beta$ lines over the same energy range.

state lifetimes [13], gas leakage up the beam line, and the target interaction length. The correction has the effect of increasing the cross sections for excited states with relatively long lifetimes. This behavior is expected since the long lifetime states will leave the target interaction region before radiating.

Finally we determined the total photon counts for each emission line. The $H\alpha$ and Doppler-shifted $H\alpha$ lines both appear with a substantial width. The OH bands also have significant width and are also comprised of many rotational peaks. Previously we fit Gaussian curves to the Balmer lines and manually fit peaks to the OH bands, and then integrated over the curves to get the total number of counts. We recently compared this method with automatic trapezoidal integration of the counts using an implementation provided by the OriginPro software, and the results were virtually identical for the Balmer lines. The automatic method also allowed for more accurate integration of the complex OH molecular bands. Because the method of automatic integration is also highly efficient, it was used instead of the Gaussian fit method.

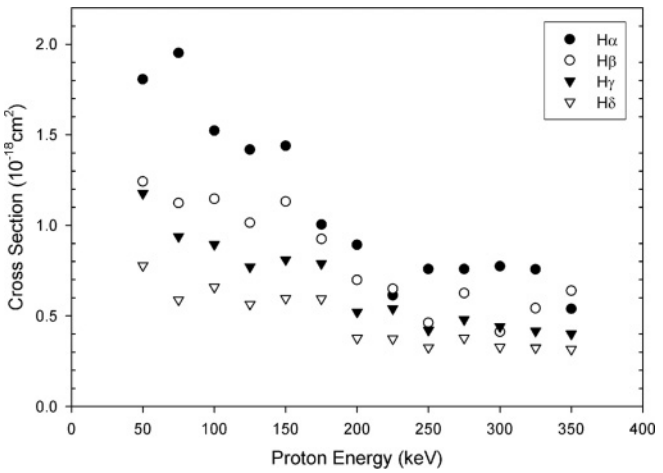

FIG. 2. Plots of all Balmer emission cross sections from the target water molecules as a function of beam energy. Values arbitrarily scaled for visualization purposes. Energy dependence is nearly identical for all four lines. Uncertainty in the data is 22%.

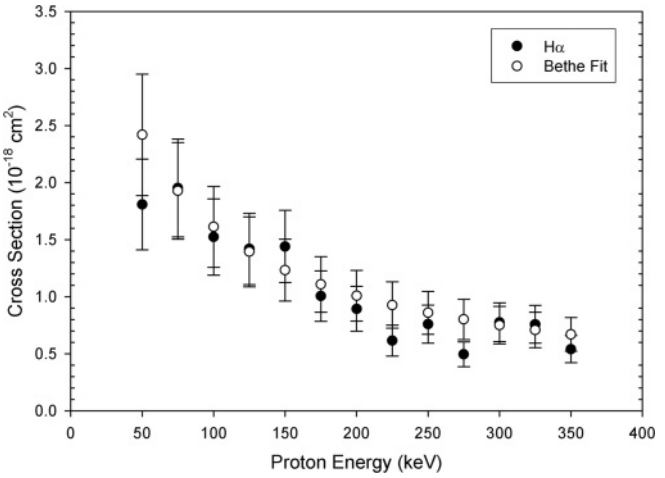

FIG. 3. $H\alpha$ target emission cross section as a function of beam energy. Also shown is a plot of the Bethe equation using M_n^2 and c_n from the experimental data.

III. RESULTS AND DISCUSSION

A. Target Balmer emission

The target emission cross sections for the Balmer lines are summarized in Fig. 2, with detailed data in Figs. 3–6. As indicated earlier, the only previous Balmer emission cross-section study (for proton impact) was done by Yousif *et al.* [9] who presented projectile and target $H\alpha$ emission cross sections in the energy range of 5 to 100 keV. Our previous work [5] indicated that our target $H\alpha$ cross section at 200 keV was not consistent with an extrapolated value on Yousif's results. This trend continues for energies from 50 to 100 keV, where

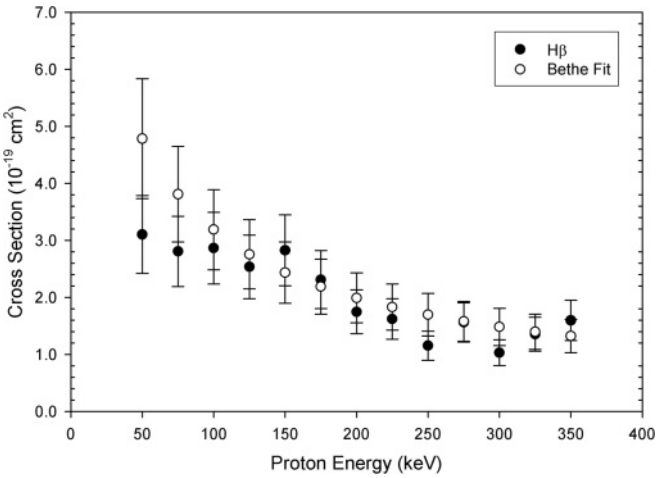

FIG. 4. $H\beta$ target emission cross section as a function of beam energy along with a plot of the Bethe equation.

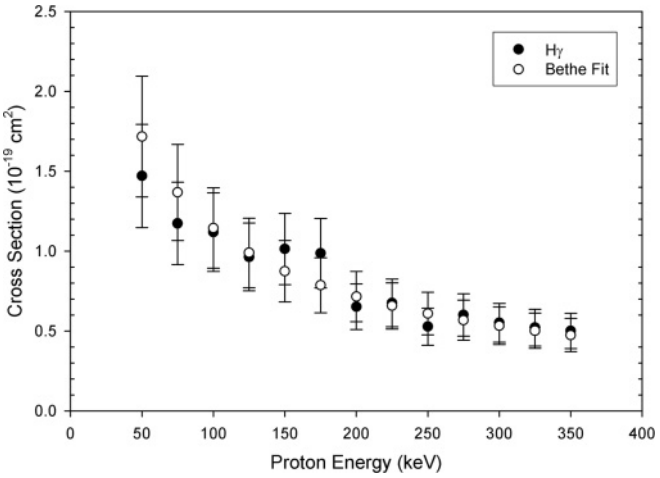

FIG. 5. $H\gamma$ target emission cross section as a function of beam energy along with a plot of the Bethe equation.

there is still a disagreement by approximately a factor of 10 at each energy. When looking at energy dependence, our $H\alpha$ cross section falls off at approximately $E^{-0.6}$, whereas the $H\alpha$ cross section in Yousif falls off at $E^{-0.52}$ in the energy range of 50 to 100 keV. We can therefore conclude that because both cross sections have similar energy dependence, the discrepancy between the two target $H\alpha$ emission data sets is most likely due to a systematic difference between measurements in the two laboratories. This systematic error may come from several different sources. (1) Normalization: Yousif normalizes their relative cross sections twice (once to their previous work, which was originally normalized to the N_2^+ cross section of Thomas). Each normalization procedure may impart substantial error. (2) Measurement of the target thickness was done directly in this experiment, while Yousif determined target thickness by reference to previously published electron capture cross sections. (3) Detector setups: Yousif utilizes an interference filter and a photomultiplier tube while we use a calibrated CCD. A slight calibration error in one or both of these setups could be responsible for a large portion of the discrepancy.

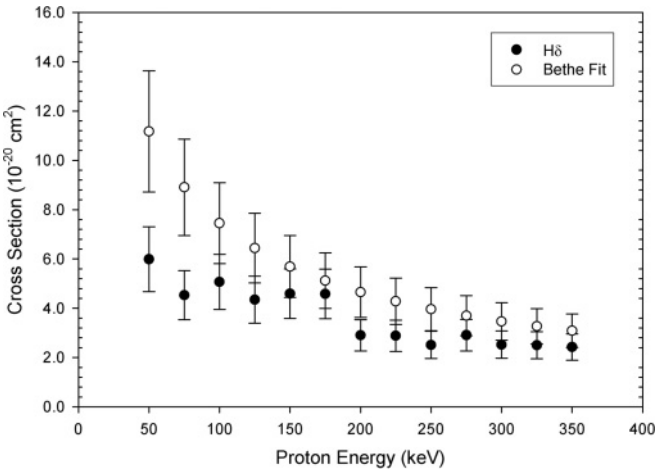

FIG. 6. $H\delta$ target emission cross section as a function of beam energy. A plot of the Bethe equation for this cross section is in substantial disagreement with the experimental data at 50 and 75 keV.

We also notice a prominent peak in Yousif's cross section at an energy of approximately 20 keV, which is in disagreement with the ionization cross-section peak at approximately 100 keV in both Gobet [6] and Rudd [14]. Our steadily decreasing cross section from 50 to 350 keV verifies the general trend in Yousif, and also indicates that photon emissions are not the result of target ionization. This is also verified by Beenaker *et al.* [15] who indicated that excited neutral fragments are produced from dissociative excitation rather than ionization.

Monce [16] performed a similar study with various ions (H^+, H_2^+, He^+) impacting on CO_2. Trends in the data showed that the target emission cross sections were dependent only on the projectile velocity rather than the projectile type. This indicated that the Bethe theory might serve as a sufficient model for the emission cross section of charged particle impact with molecules. A convenient representation of the Bethe procedure developed by Inokuti [17,18] provides the first Born approximation for the total excitation cross section:

$$\sigma_B = \frac{4\pi a_0^2 z^2}{T/\mathrm{Ry}} M_n^2 \ln\left(\frac{4c_n}{T/\mathrm{Ry}}\right), \tag{1}$$

where a_0 is the Bohr radius, z is the projectile charge, T is $1/2m_e v^2$ (m_e is the *electron* mass regardless of the projectile type), v is the projectile velocity, c_n is a constant very close to 1 (for optically allowed transitions), and M_n^2 is an element of the transition matrix. Inokuti has researched M_n^2 extensively in the past, and developed the following formula for the case of dissociative excitation [17]:

$$M_n^2 = \int_{E_n}^{\infty} \eta_n(E) \frac{df}{dE} \frac{\mathrm{Ry}}{E} dE, \tag{2}$$

where E_n is the threshold energy for dissociation, $\eta_n(E)$ is the efficiency factor for generation of specific fragments in state n, df/dE is the differential optical oscillator strength, and E is the excitation energy transferred to the molecule. We can determine the unknowns in Eq. (1) from our experimental results by using a procedure developed by Fano [19]. A linear fit to a plot of the cross section vs. the natural logarithm of the projectile energy will provide M_n^2 (the slope) and c_n (the exponential of the y intercept). Only a linear relationship of the data in a Fano plot indicates applicability of the Bethe theory for optically allowed transitions. Fano plots for all Balmer lines are illustrated in Fig. 7. There is a strong linear relationship for most cross sections, although there is substantial variance at the high energies of $H\alpha$. This is due to our experimental uncertainty. The fitting parameters generated by the Fano plots are provided in Table I and the Bethe fit curves are also shown with the experimental data in Figs. 3–6. Given this strong fit, it is reasonable to expect that it should continue for all nonrelativistic proton velocities within the range of the Born approximation. Therefore, Eq. (1) may be used along with the parameters in Table I to approximate the target emission cross sections at energies not studied in this work.

Figure 2 shows a very strong similarity in energy dependence for the Balmer lines. The ratio between any two cross

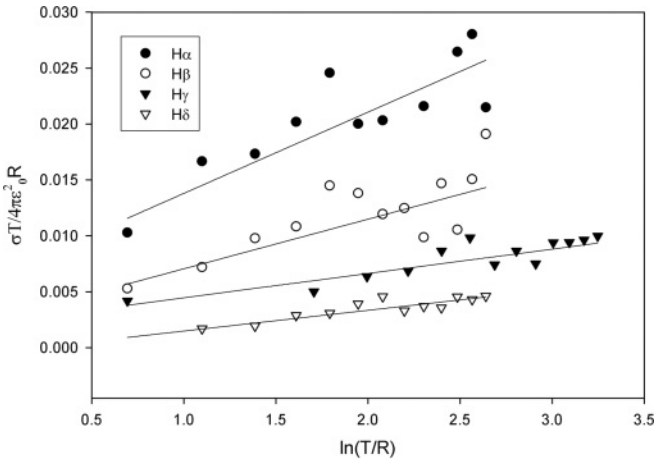

FIG. 7. Fano plots for all four Balmer emission cross sections from the target. Linear fits indicate that the Bethe theory applies. Note the $H\beta$, $H\gamma$, and $H\delta$ plots are arbitrarily scaled for convenience.

sections at any given energy should therefore be approximately equal to a constant throughout the energy range. Mohlmann and De Heer [20] also indicated this fact in their analysis of electron-H_2O collisions. According to the Bethe theory, these constants should depend only on the parameters given by Eq. (2), which includes the oscillator strength, excitation energies, and efficiencies. The value of the oscillator strength for a transition in any atom can be determined from the Einstein coefficients in the following manner [21,22]:

$$f_{ji} = \frac{2\pi\varepsilon_o m_e c^2 A_{ji} g_j}{\omega_{ji}^2 e^2 g_i} = 1.449 \times 10^8 A_{ji} \lambda_{ji}^2 \frac{g_j}{g_i}, \qquad (3)$$

where ε_o is the permittivity of free space in F/m^2, c is the speed of light in m/s, m_e is the mass of the electron in kg, A_{ji} is the probability of transition in units of 10^8 s^{-1}, ω_{ji} is the angular frequency of the transition in s^{-1}, e is the charge of the electron in C, λ_{ji} is the wavelength of transition is Ångstroms, g_j is the degeneracy of the upper energy level, and g_i is the degeneracy of the lower energy level. By computing the experimental ratios for all Balmer emission cross sections, we found the following simple approximation:

$$\frac{\sigma_{k-2}}{\sigma_{j-2}} \approx \left(\frac{f_{k-2}}{f_{j-2}}\right). \qquad (4)$$

This ratio is unexpected, especially when considering the analysis of both Beenaker *et al.*, and Mohlmann and De Heer. The former work showed that when the water molecule dissociates, there are several different pathways, each with different onset energies. $H\alpha$ emission can arise from dissociation into H($n = 3$) + OH($A\,^2\Pi$), H($n = 3$) + OH($X\,^2\Pi$), or H($n = 3$) + H($n = 1$) + O($2p^4\ ^3P$), while $H\beta$ and $H\gamma$ emission arise from only H + OH($X\,^2\Pi$). The latter work indicated that Stark mixing due to electric field perturbation (from both intermolecular or intramolecular fields created during dissociation) changes the branching ratio of radiative decay by hydrogen atoms. This would therefore prohibit the ability of using Balmer emission intensities or oscillator strengths to analyze the emission cross sections. The trends in our results indicate the following: (1) For our approximation to hold, the H + OH($X\,^2\Pi$) pathway must be the dominant process and (2) Stark mixing does not have an appreciable effect on these emissions. We also note that when analyzing the experimental results of both Beenaker *et al.* and Mohlmann and De Heer (for electron impact of H_2O at 300 and 100 eV impact energy), Eq. (4) generally holds within the uncertainty ranges. Figure 8 shows the result of applying our approximation for just a few of the Balmer lines in this work. Figure 9 shows the previously determined electron impact cross sections for $H\alpha$ and $H\beta$ along with the $H\beta$ cross section calculated using Eq. (4).

TABLE I. Values of M_n^2 and c_n for calculation of the Bethe cross section for all four Balmer lines and the OH bands at extended energies.

Species	$M_n{}^2$	$\delta M_n{}^2$	c_n	δc_n
$H\alpha$	0.006 62	0.001 46	1	0.01
$H\beta$	0.001 31	0.0002 73	1	0.001
$H\gamma$	0.000 470	0.000 098 0	1	0.0001
$H\delta$	0.000 306	0.000 049 0	1	0.0001
OH (1,0)	0.001 91	0.000 420	1	0.001
OH (0,0)	0.0192	0.004 20	1	0.01

B. Projectile Balmer emission

In Fig. 10 we present the cross sections for Balmer emission from the projectile. Note that the Doppler-shifted lines decrease substantially in magnitude at higher energies (as shown in Fig. 1). Eventually these lines blend in with the background noise, making then much more difficult to integrate accurately. As a result, we increased the experimental error in the cross sections to 40% at a threshold determined by the line strength at a given energy. The $H\delta$ Doppler-shifted lines were not clearly visible throughout the entire energy range. Since we did not study emission from charge transfer in our previous work [5], we present a general overview of

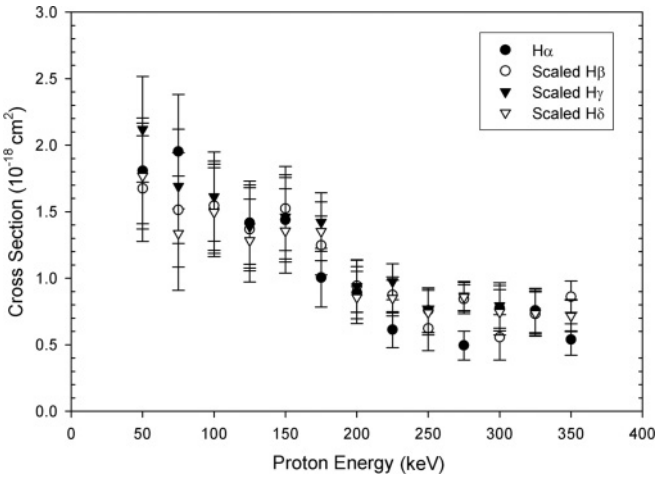

FIG. 8. Plot showing the results of using Eq. (4) to scale the $H\beta$, $H\gamma$, and $H\delta$ cross sections with respect to $H\alpha$.

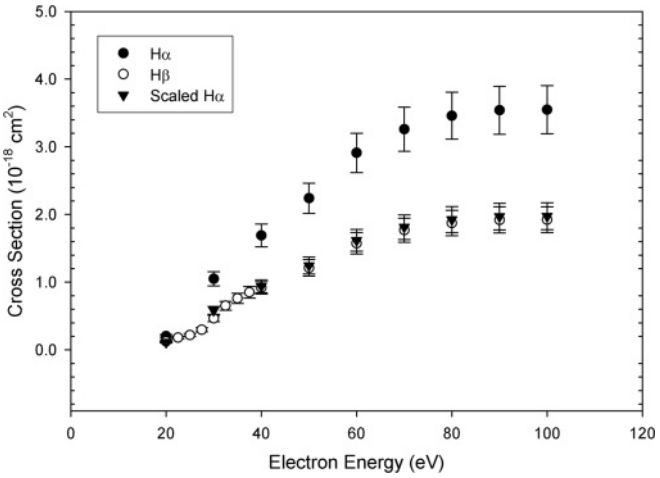

FIG. 9. A plot of the $H\alpha$ [20], and $H\beta$ [15] target emission cross sections for electron impact of H_2O. Also shown is the result of applying Eq. (4) to scale $H\alpha$ with respect to $H\beta$. Most of the experimental $H\beta$ data points are not clearly visible due to overlap from the scaled $H\alpha$ cross section.

the possible interaction processes here. For single electron capture, the following processes are possible [23]:

$$H^+ + H_2O \rightarrow H^* + H_2O^+, \tag{5a}$$

$$H^+ + H_2O \rightarrow H^* + (H_2O^+)^*, \tag{5b}$$

where process (5b) is single electron capture with excitation. Since the unstable ions of H_2O do not travel into our target cell, we only observe emission from excited neutral hydrogen. We also theorize that double electron capture may also occur, in which Hydrogen anions are formed via the capture of two electrons from the same molecular orbital. The cross section for the production of hydrogen anions from collisions of protons with helium atoms has been studied in depth [24]. When Gobet [14] analyzed the product ion channels for collisions of protons with water molecules, no evidence for negatively charged ions were found. Unfortunately, we also cannot draw any further conclusions of the production of H^-, as it is a quantum system with a single bound state [25], thus no photon emission can be observed.

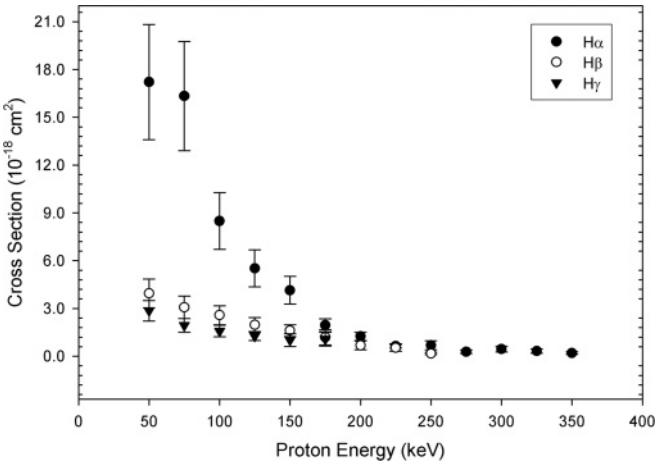

FIG. 10. Plot of the projectile emission cross sections as a function of beam energy. The uncertainties are as follows: for $H\alpha$ the uncertainty is 22% from 50–225 keV and 40% from 250–350 keV. For $H\beta$ the uncertainty is 22% from 50–150 keV and 40% from 175–250 keV. For $H\gamma$ the uncertainty is 22% from 50–125 keV and 40% from 150–175 keV.

The capture cross section cannot be described by the Bethe theory due to the large momentum transfer that occurs during charge exchange between protons and molecules. The charge-transfer process is actually quasielastic in nature [26]. Houamer *et al.* [27] have indicated that the full plane-wave first-Born approximation (PWFBA) can be used to model these quasielastic charge-transfer processes. For the water molecule they utilized a single-center Hartree-Fock wave function (centered on oxygen) and a frozen core approximation for the electrons to calculate the absolute total capture cross section for proton impact. The results for H_2O fail to replicate the leveling off of the capture cross section between 5 and 50 keV, as indicated by the data of Yousif. This is because the PWFBA is not valid at low energies. Nevertheless, the PWFBA can still illustrate the physics behind the capture processes at moderate to high energies. Houamer *et al.* conclude that only the outermost orbitals of H_2O are involved in capture processes up to approximately 500 keV, and after this energy threshold the inner $1a^1$ orbital begins to contribute to capture.

We can also compare our projectile emission cross sections to those of Yousif *et al.* At 50 keV our $H\alpha$ cross section is 1.72×10^{-17} cm^2, compared to 8.37×10^{-18} cm^2. These values are somewhat closer than those for target emission; however, the two data sets are still inconsistent when considering the uncertainty ranges. Yousif *et al.* demonstrates that the $H\alpha$ capture cross-section levels off at about 20 keV and starts decreasing somewhat rapidly at about 50 keV. Our data confirms this general trend, and in the overlapping energy range of the data sets the energy dependence is similar ($E^{-0.96}$ and $E^{-1.05}$).

As stated earlier, we applied a correction factor to the photon counts of Doppler-shifted lines to account for the lifetimes of the radiating states. Application of the correction factor results in cross-sections that are dissimilar in energy dependence. At first glance this would indicate that these cross sections are not scalable using the oscillator strength ratios. However, when analyzing the emission from radiating hydrogen atoms within the target cell only, the cross sections do have similar energy independence. Despite the fact that electron capture processes cannot be described by the Bethe theory, the Balmer emissions within view of our CCD have intensities that are generally proportional to corresponding oscillator strengths. Therefore, to calculate the ratio of any two projectile Balmer emission cross sections, we can combine our correction factor [12] with Eq. (4) to generate the following approximation:

$$\frac{\sigma_{k-2,\mathrm{cap}}}{\sigma_{j-2,\mathrm{cap}}} \approx \left(\frac{f_{k-2}}{f_{j-2}}\right) \frac{[(k + 1/v\tau_{k-2})(1 - e^{-l/v\tau_{j-2}})]}{[(k + 1/v\tau_{j-2})(1 - e^{-l/v\tau_{k-2}})]}, \tag{6}$$

where v is the proton velocity, k is a diffusion constant related to the change in gas density over beam line distance (2.14), τ is A^{-1} for the given transition, and l is the target interaction length (0.0481 m). Figure 11 shows an example of applying the above equation to the $H\beta$ and $H\gamma$ cross sections. The

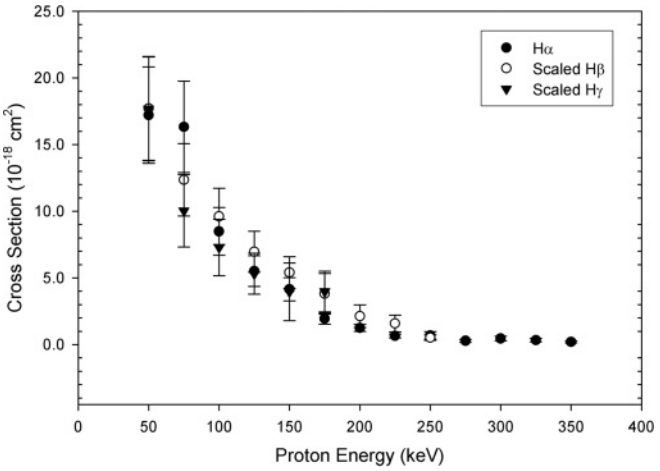

FIG. 11. Plot showing the results of using Eq. (6) to scale the $H\beta$, $H\gamma$, and $H\delta$ projectile emission cross sections with respect to $H\alpha$.

approximation is generally within the uncertainty range of the experimental results, however it tends to deviate slightly at higher energies. A significant portion of this deviation may be due to the greater uncertainty in measuring the Doppler-shifted lines, as they are substantially less intense than the target emissions at high energy.

C. Target OH emission

The results for the $A\,^2\Sigma^+ - X\,^2\Pi$ 285 nm (1,0) and 315 nm (0,0) OH emission cross sections are provided in Figs. 12 and 13. In our previous work we determined the (0,0) emission cross section at 200 keV to be 8.9×10^{-19} cm^2, which is 56% lower than our current measurement at the same energy. We believe this may be due to the fact that a manual peak-fitting procedure was applied to the OH molecular bands in the previous work. As stated earlier, we now use the method of automatic trapezoidal integration, which takes into account even the smallest rotational peaks within the vibrational band. We also compared our (0,0) emission cross section to that of Nussbaum and Cathers [10], and concluded that their value of

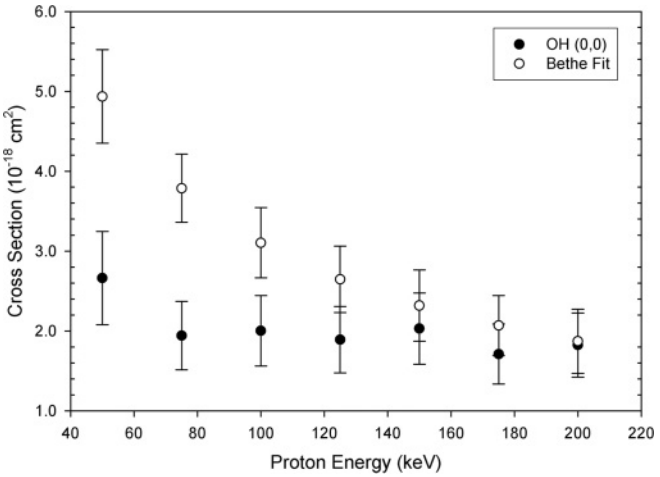

FIG. 12. OH (0,0) target emission cross section as a function of beam energy. Also shown is a plot of the Bethe equation which is inconsistent with the experimental data. Uncertainty is 20%.

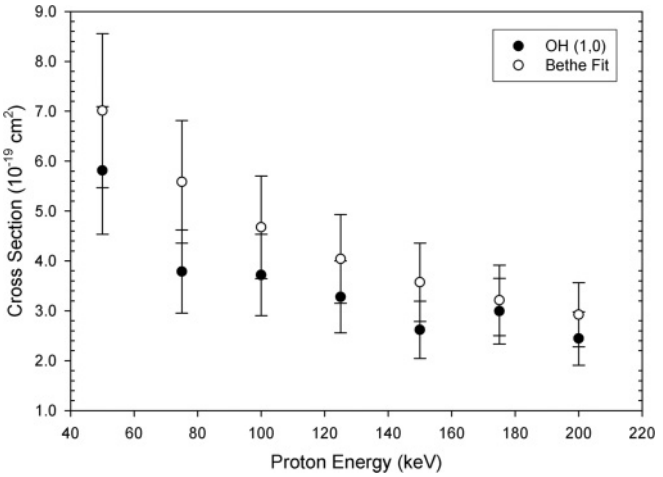

FIG. 13. OH (1,0) target emission cross section as a function of beam energy. Also shown is a plot of the Bethe equation. Unlike the (0,0) emission band, the Bethe fit here is consistent with all data points. Uncertainty is still 20%.

1.75×10^{-19} cm^2 for the averaged cross section at 200 keV was incorrect due to error in the normalization value. We originally stated that the average of their 150 and 250 keV relative cross sections should have been normalized to the less uncertain 200 keV $N_2{}^+$ cross section of Thomas [28]. This however was incorrect because the relative cross sections (at all energies) in Nussbaum were determined using a comparison to their own measurement of $N_2{}^+$ emission at 50 keV. When their original values (normalized to Dufay *et al.* [29]) are used, the data are in agreement within the uncertainty range. When using our measurements of $N_2{}^+$ emission for the normalization of the relative cross sections in Nussbaum, the results are also consistent within the uncertainties. Regardless of the values used for normalization, the two data sets have similar energy dependence, $E^{-0.33}$ and $E^{-0.30}$, the latter for the current work.

Fano plots in Fig. 14 indicate that the Bethe theory also applies to the vibrational emissions of OH. The Beth-fit curves are shown in Figs. 12 and 13. Clearly the fit curve for the (0,0)

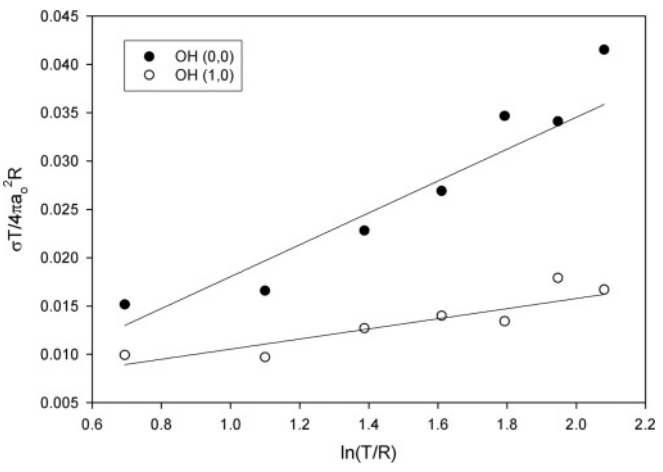

FIG. 14. Fano plots for both OH emission cross sections. Linear fits indicate that the Bethe theory applies. Note the (1,0) data is scaled by a factor of 3.

band is inconsistent with our experimental results at lower energies. This is most likely due to the fact that fewer data points were recorded for the OH bands, resulting in a Fano fit that has substantially more uncertainty. Also, we note that when using the oscillator strengths given in Ref. [30], Eq. (4) does not hold. Further theoretical and possibly experimental work is necessary to determine why this is the case.

IV. CONCLUSIONS

We have determined the Balmer $\alpha-\delta$ and excited OH emission cross sections from proton impact of H_2O in an energy range of 50 to 350 keV. Fano plots indicated that the Bethe theory accurately describes the emission cross section from collisions with the target. We also showed that it is possible to approximate the ratio of any two Balmer emission cross sections by computing the ratio of their respective oscillator strengths regardless of the impact energy. This relation applies to the previously published data for electron impact as well. Doppler-shifted Balmer lines indicated emission from the projectile due to electron capture processes occurring before the target slit. These processes do not follow the Bethe theory, as large momentum transfer occurs during projectile-target interaction. Nevertheless, we showed that the ratio of any two Balmer emission cross sections from the projectile can be approximated by a corrected ratio of the respective oscillator strengths. By performing detailed comparisons with previously published results, we determined that our cross sections generally decrease with increasing energy in a similar manner, despite some discrepancies between the magnitudes of the data sets. Finally, we provide the parameters necessary to calculate the Bethe cross sections for all target emissions at nonrelativistic energies not studied in this work.

ACKNOWLEDGMENTS

Student support was provided by the Keck Undergraduate Science Program, Connecticut College. We also thank the referees for their helpful comments.

[1] F. Gobet, B. Farizon, M. Farizon, M. J. Gaillard, M. Carre, M. Lezius, P. Scheier, and T. D. Mark, Phys. Rev. Lett. **86**, 3751 (2001).
[2] M.Galand and S. Chakrabarti, J. Atm. Solar-Terr. Phys. **68**, 1488 (2006).
[3] L. Moore, A. F. Nagy, A. J. Kliore, I. Müller-Wodarg, J. D. Richardson, and M. Mendillo, Geophys. Res. Lett. **33**, L22202 (2006).
[4] C. Paranicas, D. G. Mitchell, S. M. Krimigis, D. C. Hamilton, E. Roussos, N. Krupp, G. H. Jones, R. E. Johnson, J. F. Cooper, and T. P. Armstrong, Icarus **197**(2), 519 (2008).
[5] M. N. Monce, S. Pan, N. L. Radeva, and J. L. Pepper, Phys. Rev. A **79**, 012704 (2009).
[6] F. Gobet, S. Eden, B. Coupier, J. Tabet, B. Farizon, M. Farizon, M. J Gaillard, M. Carre, S. Ouaskit, T. D. Mark, and P. Scheier, Phys. Rev. A **70**, 062716 (2004).
[7] H. Luna *et al.*, Phys. Rev. A **75**, 042711 (2007).
[8] M. A Bolorizadeh and M.E. Rudd, Phys. Rev. A **33**, 882 (1986).
[9] F. B. Yousif, J. Geddes, and H. B. Gilbody, J. Phys. B **19**, 217 (1986).
[10] G. H. Nussbaum and A. R. Cathers, J. Chem. Phys. **65**, 4170 (1976).
[11] E. W. Thomas, *Excitations in Heavy Particle Collisions* (Wiley-Interscience, New York, 1972).
[12] T. F. Ammirati, M. N. Monce, D. Tadesse, P. M. Luthy, and N. Alvarado, J. Geophys. Res. **110**, A04214 (2005).
[13] W. L Wiese, M. W. Smith, and B. M. Glennon, Natl. Stand. Ref. Data Ser., Natl. Bur. Stand. **4**, Category 3 (1966).
[14] M. E. Rudd, T. V Goffe, R. D DuBois, and L. H. Toburen, Phys. Rev. A **31**, 492 (1985).
[15] C. I. M. Beenakker, F. J. de Heer, H. B. Krop, and G. R. Mohlmann, Chem. Phys. **6**, 445 (1974).
[16] M. N. Monce, Phys. Rev. A **38**, 3351 (1988).
[17] M. Inokuti, Rev. Mod. Phys. **43**, 297 (1971).
[18] M. Inokuti and Y.-K. Kim, Phys. Rev. A **1**, 1132 (1970).
[19] U. Fano, Phys. Rev. **95**, 1198 (1954).
[20] G. R. Mohlmann and F. J. de Heer, Chem. Phys. **40**, 157 (1979).
[21] R. C. Hilborn, Am. J. Phys. **50**, 982 (1982).
[22] W. C. Martin and W. L. Wiese, J. Res. Natl. Inst. Stand. Technol., Atomic Spectroscopy Online Database (2010).
[23] S. Mada, K. Hida, M. Kimura, L. Pichl, H.-P. Liebermann, Y. Li, and R. J. Buenker, Phys. Rev. A **75**, 022706 (2007).
[24] K. Roy, S. C. Mukherjee, and D. P. Sural, Phys. Rev. A **13**, 987 (1976).
[25] C. E. Strauss, D. J. Funk, X. M. Zhao, A. Stintz, D. Rislove, M. Gulley, and H. C Bryant, DOE Office of Scientific and Technical Information, LA-UR-97-2322 (1997).
[26] E. Weigold and I. E McCarthy, *Electron Momentum Spectroscopy* (Kluwer Academic, New York, 1999).
[27] S. Houamer, Y.V. Popov, and C. D. Cappello, Phys. Lett. A **373**, 48, 4447 (2009).
[28] E. W. Thomas, G. D. Bent, and J. L. Edwards, Phys. Rev. **165**, 32 (1968).
[29] M. Dufay, J. Desesquelles, M. Druetta, and M. Eidelsberg, Ann. Geophys. **22**, 614 (1966).
[30] J. Luque and D. R. Crosley, J. Chem. Phys. **109**, 439 (1998).